SPECIAL TOPIC — International Conference on Nanoscience & Technology, China 2013

Large coercivity and unconventional exchange coupling in manganese-oxide-coated manganese–gallium nanoparticles*

Feng Jun-Ning(冯俊宁), Liu Wei(刘 伟)†, Geng Dian-Yu(耿殿禹), Ma Song(马 嵩), Yu Tao(余 涛), Zhao Xiao-Tian(赵晓天), Dai Zhi-Ming(代志明), Zhao Xin-Guo(赵新国), and Zhang Zhi-Dong(张志东)

Shenyang National Laboratory for Materials Science and International Center for Materials Physics, Institute of Metal Research, Chinese Academy of Sciences, Shenyang 110016, *China*

(Received 4 September 2013; revised manuscript received 20 March 2014; published online 10 June 2014)

The microstructures and magnetic properties of nanoparticles, each composed of an antiferromagnetic (AFM) manganese-oxide shell and a ferromagnetic-like core of manganese–gallium (MnGa) compounds, are studied. The core-shell structure is confirmed by transmission electron microscope (TEM). The ferromagnetic-like core contains three kinds of MnGa binary compounds, i.e., ferrimagnetic (FI) $D0_{22}$-type Mn_3Ga, ferromagnetic (FM) Mn_8Ga_5, and AFM $D0_{19}$-type Mn_3Ga, of which the first two correspond respectively to a hard magnetic phase and to a soft one. Decoupling effect between these two phases is found at 1ow temperature, which weakens gradually with increasing temperature and disappears above 200 K. The exchange bias (EB) effect is observed simultaneously, which is caused by the exchange coupling between the AFM shell and FM-like core. A large coercivity of 6.96 kOe (1 Oe = 79.5775 A·m^{-1}) and a maximum EB value of 0.45 kOe are achieved at 300 K and 200 K respectively.

Keywords: nanoparticle, core-shell structure, exchange coupling

PACS: 75.75.–c, 71.70.Gm **DOI:** 10.1088/1674-1056/23/8/087503

1. Introduction

Rare-earth (RE) permanent magnets with large values of magnetocrystalline anisotropy (K_u), saturation magnetization (M_S), and magnetic energy product $(BH)_{max}$ are widely used in various advanced electromagnetic devices such as traction motors of hybrid and pure electric vehicles and wind generators.[1,2] But the applications of RE permanent magnets are being limited due to the high cost and the chemical instabilities of RE elements. There is economic and scientific interest in developing new permanent magnetic materials containing no RE elements.[3,4] High-performance permanent magnets must have a large K_u, a high M_S and a high Curie temperature (T_C). Mn-based compounds such as MnAl,[5] Mn_xGa,[6–15] and MnBi[16] are good candidates for new permanent-magnetic materials free of RE elements. In recent years, there is growing attention to Mn_xGa compounds because of their many outstanding magnetic properties. The magnetic properties of binary Mn_xGa are tunable in a wide composition range. The crystal structures of Mn_xGa are of tetragonal $L1_0$-type and $D0_{22}$-type for $0.76 \leq x \leq 1.8$ and $2 \leq x < 3$,[7,8,11] respectively. The theoretically expected K_u, M_S, and $(BH)_{max}$ of $L1_0$-type MnGa are 26 Merg/cc, 845 emu/cc, and 28.2 MGOe, while the values for $D0_{22}$-type MnGa are 20 Merg/cc, 305 emu/cc, and 3.67 MGOe respectively.[6–9] The structural and magnetic properties of Mn_xGa have been investigated on bulk materials,[10,11] melt-spun ribbons[17] and thin films grown on various substrates including Si (Si/SiO_2),[12,13] GaAs,[6,14] GaSb,[13] MgO,[15] etc. Epitaxial Mn_xGa films exhibit excellent perpendicular anisotropy when grown on lattice-matched substrates. Until now, the research about nanoparticle-shaped Mn_xGa alloys has been seldom reported. In the present paper, we investigate the magnetic properties and exchange coupling in the manganese-oxide-coated Mn–Ga nanoparticles with a core-shell structure prepared by the arc-discharge technique.

2. Experiments

The manganese-oxide-coated Mn–Ga nanoparticles were prepared by the arc-discharge technique.[18] A $Mn_{60}Ga_{40}$ ingot to be evaporated was used as the anode, and a tungsten needle was served as the cathode. The anode was placed in a water-cooled copper crucible. The distance between the anode and the cathode was about 1.5 mm. The base pressure of the chamber was better than 5.0×10^{-3} Pa. High purity argon was chosen as the source of plasma gas, which was kept at a pressure of 2.0×10^4 Pa. After the arc was ignited, a current of 60 A was maintained with a potential sustained in a range of 8 V–10 V between the cathode and the anode. Subse-

*Projected supported by the National Basic Research Program of China (Grant No. 2010CB934603), the National High Technology Research and Development Program of China (863 Program) (Grant No. 2011AA03A402), and the National Natural Science Foundation of China (Grant Nos. 50931006, 51271177, and 51271179).

†Corresponding author. E-mail: wliu@imr.ac.cn

© 2014 Chinese Physical Society and IOP Publishing Ltd

quently, Mn–Ga alloy nanoparticles were formed on the water-cooled wall of the work chamber. Then the residual gases were pumped out after turning off the arc, and pure argon gas with a pressure of 1.0×10^4 Pa was introduced for passivating the products for about 24 h. Manganese-oxide shells were formed on their surfaces when the nanoparticles were exposed in air. Thus manganese-oxide-coated Mn–Ga nanoparticles with a core–shell structure were obtained. The products on the top of the chamber were collected in air.

The crystal structures of the nanoparticles were investigated by means of X-ray diffraction (XRD) through a D/max2500PC diffractometer with Cu Kα radiation at 50 kV and 300 mA. The size distribution, morphology, and structure of the manganese-oxide-coated Mn–Ga nanoparticles were investigated by a Tecnai G^2F20 transmission electron microscopy (TEM) with an emission voltage of 200 kV. The magnetic properties of the manganese-oxide-coated Mn–Ga nanoparticles were measured at different temperatures after field cooling (FC) from 300 K in a field of 50 kOe using a superconducting quantum interference device (SQUID, Quantum Design MPMS-7) magnetometer.

3. Results and discussion

Figure 1 shows the XRD patterns of the manganese-oxide-coated Mn–Ga nanoparticles. It is clear that Mn_8Ga_5, Mn_3Ga, and MnO coexist in the sample. The crystal structure of Mn_8Ga_5, which is also called ζ phase, is primitive cubic and it is ferromagnetic (FM) compound with a T_C of about 210 K.[19] The Mn_3Ga phase combines a tetragonal $D0_{22}$-type Mn_3Ga and a hexagonal $D0_{19}$-type one, which are marked as o and o′ respectively in Fig. 1. The former is ferrimagnetic (FI) compound with a T_C of about 770 K,[20] and the latter is antiferromagnetic (AFM) compound with a Néel temperature (T_N) of about 470 K.[21]

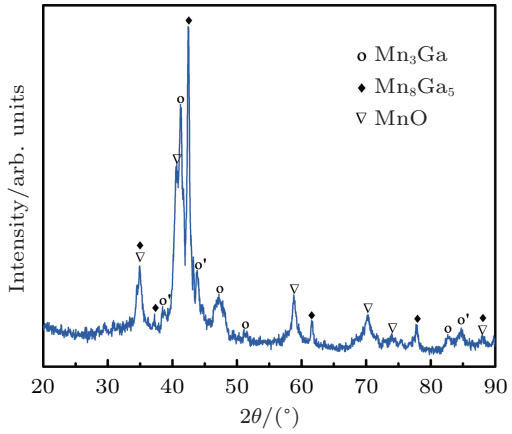


Fig. 1. (color online) XRD patterns of the manganese-oxide-coated Mn–Ga nanoparticles.

TEM images of the manganese-oxide-coated Mn–Ga nanoparticles are shown in Fig. 2. A low magnification TEM image in Fig. 2(a) shows that the nanoparticles present a good dispersion property and a uniform size distribution. The cores of the nanoparticles are about 40 nm–50 nm in diameter and the thickness of the shells is about 5 nm. The core–shell structures of the present nanoparticles are observed in the high-resolution TEM image (see Fig. 2(b)). From the results of the energy dispersive spectrometer (EDS), the atomic percentages of Mn to Ga in the core and the Mn to O in the shell are both very close to 1:1. The existence of AFM MnO in the shell is confirmed by the EDS results, which is consistent with the XRD result. In addition, the O element and Ga element are not observed in the cores and shells respectively. Since the nominal composition ratios of Mn to Ga in Mn_3Ga and Mn_8Ga_5 are both greater than 1:1, some pure nonmagnetic Ga elements may exist in the nanoparticles.

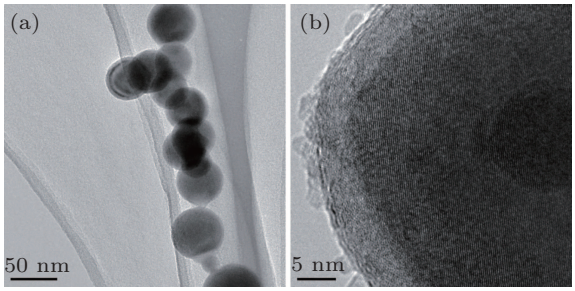


Fig. 2. (a) TEM image and (b) high-resolution TEM image of the manganese-oxide-coated Mn–Ga nanoparticles.

The magnetic hysteresis loops of the manganese-oxide-coated Mn–Ga nanoparticles are measured at different temperatures after FC procedure from 300 K at a field of 50 kOe, and the results are shown in Fig. 3. Obvious shoulders are observed in the hysteresis loops at the measuring temperatures below 200 K, which may originate from the decoupling between two magnetic phases. The ζ phase and the tetragonal $D0_{22}$-type Mn_3Ga correspond to the magnetically soft phase and the hard phase respectively. $D0_{22}$-Mn_3Ga probably has a huge coercive field (H_C) at very low temperature, which means that the K_u of $D0_{22}$-Mn_3Ga is relatively large and has a nonlinear dependence with temperature. The hysteresis loops measured above 200 K are more like a single-phase loop. The reason is that the ζ phase becomes paramagnetic above 200 K. As the applied field increases, an upward trend is kept in each of all hysteresis loops, which indicates that it is hard to saturate the magnetization of the nanoparticles. This is a common feature of the nanoparticle-system consisting of an AFM component.

As a result of the exchange coupling between the FM-like core and the AFM shell, the exchange bias (EB) effect is observed in the manganese-oxide-coated Mn–Ga nanoparticles. The temperature dependences of H_C and EB field (H_E) are shown in Fig. 4. A positive temperature coefficient of H_C is observed as a result of the hard–soft exchange coupling.

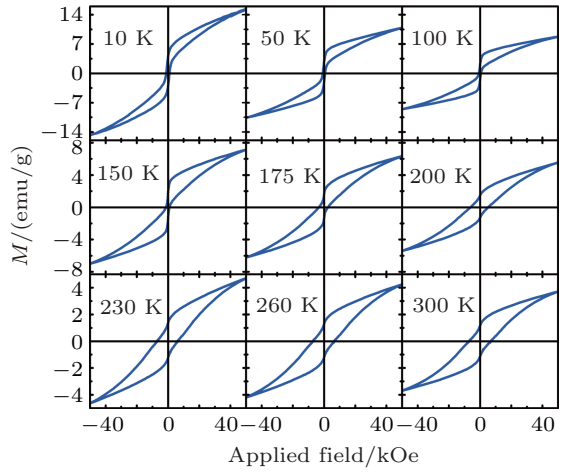


Fig. 3. (color online) Hysteresis loops measured at different temperatures after FC at a field of 50 kOe for the manganese-oxide-coated Mn–Ga nanoparticles.

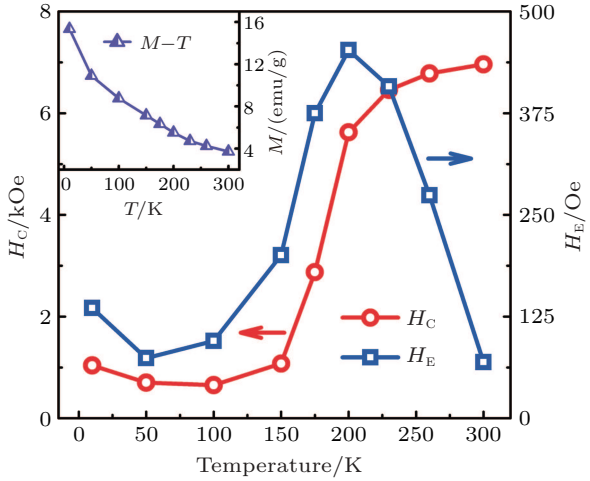


Fig. 4. (color online) Temperature dependences of H_C and H_E of the manganese-oxide-coated Mn–Ga nanoparticles, with the inset showing the temperature dependence of the magnetization measured at 50 kOe.

At the temperatures below 200 K, H_C is mainly contributed by the magnetically-soft ζ phase. After the ζ phase changes into paramagnetic phase above 200 K, the hard phase gradually plays a decisive role in the H_C of the nanoparticles. The manganese-oxide-coated Mn–Ga nanoparticles present a rather large coercivity of 6.96 kOe at 300 K. The large coercivity should be attributed to the small size of the nanoparticles and the exchange coupling between the FI $D0_{22}$-Mn_3Ga and the AFM $D0_{19}$-Mn_3Ga. The possibility that the H_C continuously increases with increasing temperature cannot be excluded. If the Mn–Ga system truly has this positive temperature coefficient of coercivity, this material can be widely used in rare-earth-free permanent magnets. The EB effect is observed from 10 K to 300 K, and a peak of H_E of 0.45 kOe is found at 200 K in our system. It is noted that the AFM MnO and $D0_{19}$-Mn_3Ga are ordered at $T_N = 119$ K and 470 K respectively. So the maximum H_E results from the exchange coupling between FI $D0_{22}$-Mn_3Ga and AFM $D0_{19}$-Mn_3Ga. The H_E peak is corresponding to the T_C of the ζ phase. It is concluded that the maximum of exchange coupling strength is achieved at 200 K. The temperature dependence of the magnetization at a field of 50 kOe is shown in the inset of Fig. 4, showing that the magnetization decreases linearly with increasing temperature. A maximum value of magnetization is 15.35 emu/g at 10 K.

Figure 5 shows the temperature dependences of the FC and zero-field-cooling (ZFC) magnetizations under a field of 50 Oe for the manganese-oxide-coated Mn–Ga nanoparticles. A prominent irreversibility is observed between FC and ZFC curves. A similar bifurcation between the ZFC and FC curves has been observed in other core–shell nanoparticle-systems as well,[22,23] which is an evidence for the existence of a thermal irreversibility of magnetization. The bifurcation between FC and ZFC curves vanishes under a magnetic field of 10 kOe (see the inset of Fig. 5). The $T_C = 187$ K of the ζ phase is obtained. The T_C of $D0_{22}$ Mn_3Ga cannot be achieved in our experiment, because it is beyond the measurement range.

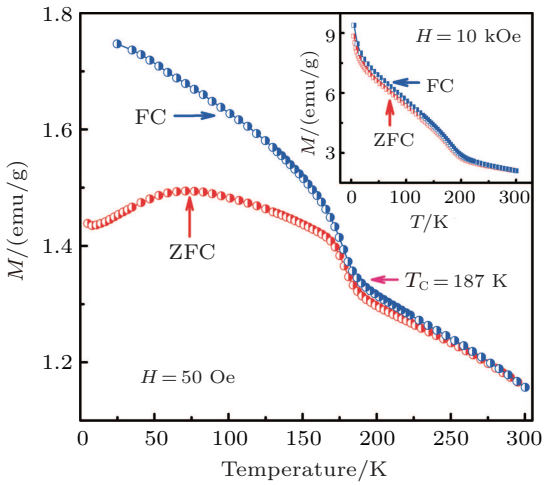


Fig. 5. (color online) Temperature dependences of the FC and ZFC magnetizations under a field of 50 Oe and 10 kOe (in inset) for the manganese-oxide-coated Mn–Ga nanoparticles.

4. Conclusions

The manganese-oxide-coated Mn–Ga nanoparticles with AFM shells and FM-like cores are synthesized by the arc-discharge technique from an $Mn_{60}Ga_{40}$ alloy ingot. The microstructures and magnetic properties of the nanoparticles are studied. Decoupling effects at low temperature due to the coexistence of the hard- and soft-magnetic phases are observed, which disappears above 200 K. As a result of the exchange coupling between the AFM component and FM component, the EB effect is found simultaneously. A large H_C of 6.96 kOe and maximum H_E of 0.45 kOe are achieved at 300 K and 200 K respectively.

References

[1] Herbst J F 1991 *Rev. Mod. Phys.* **163** 819

[2] Coey J M D 2002 *J. Magn. Magn. Mater.* **248** 441
[3] U.S. Department of Energy, Critical Materials Strategy, 2011
[4] Editorial 2011 *Nat. Mater.* **10** 157
[5] Koch A J J, Hokkeling P, Steeg M G and Vos K J 1960 *J. Appl. Phys.* **31** S75
[6] Zhu L J, Nie S H, Meng K K, Pan D, Zhao J H and Zheng H Z 2012 *Adv. Mater.* **24** 4547
[7] Mizukami S, Wu F, Sakuma F, Walowski J, Watanabe D, Kubota T, Zhang X, Naganuma H, Oogane M, Ando Y and Miyazaki T 2011 *Phys. Rev. Lett.* **106** 117201
[8] Mizukami S, Kubota T, Wu F, Zhang X, Miyazaki T, Naganuma H, Oogane M, Sakuma A and Ando Y 2012 *Phys. Rev. B* **85** 014416
[9] Sakuma A 1998 *J. Magn. Magn. Mater.* **187** 105
[10] Balke B, Fecher G H, Winterlik J and Felser C 2007 *Appl. Phys. Lett.* **90** 152504
[11] Winterlik J, Balke B, Fecher G H, Felser C, Alves M C M, Bernardi F and Morais J 2008 *Phys. Rev. B* **77** 054406
[12] Zha C L, Dumas R K, Lau J W, Mohseni S M, Sani S R, Golosovsky I V, Monsen A F, Nogués J and Åkerman J 2011 *J. Appl. Phys.* **110** 093902
[13] Feng W, Thiet D V, Dung D D, Shin Y and Cho S 2010 *J. Appl. Phys.* **108** 113903
[14] Tanaka M, Harbison J P, DeBoeck J, Sands T, Philips B, Cheeks T L and Keramidas V G 1993 *Appl. Phys. Lett.* **62** 1565
[15] Kurt H, Rode K, Venkatesan M, Stamenov P and Coey J M D 2011 *Phys. Rev. B* **83** 040205
[16] Heikes R R 1955 *Phys. Rev.* **99** 446
[17] Saito T and Nishimura R 2012 *J. Appl. Phys.* **112** 083901
[18] Zhang Z D 2007 *J. Mater. Sci. Technol.* **23** 1
[19] Tsuboya I and Sugihara M 1963 *J. Phys. Soc. Jpn.* **18** 1096
[20] Kübler J 2006 *J. Phys.: Condens. Matter* **18** 9795
[21] Niida H, Hori T and Nakagawa Y 1983 *J. Phys. Soc. Jpn.* **52** 1512
[22] Yusuf S M, Manna P K, Shirolkar M M, Kulkarni S K, Tewari R and Dey G K 2013 *J. Appl. Phys.* **113** 173906
[23] Si P Z, Brück E, Zhang Z D, Tegus O, Zhang W S, Buschow K H J and Klaasse J C P 2005 *Mater. Res. Bull.* **40** 29